Numerical Assessment of the Maximum Operating Pressure for SAGD Projects Considering the Effects of Anisotropy and Natural Fractures

Ehsan Rahmati, Alireza Nouri, Vahidoddin Fattahpour, Japan Trivedi, University of Alberta

Abstract

There has been an increasing awareness of the importance of caprock integrity during Steam Assisted Gravity Drainage (SAGD) operations. However, mathematical tools that have been developed for caprock integrity studies have not incorporated an important characteristic of cap shales, which is the intrinsic anisotropy and structural anisotropy caused by the natural fractures (NFs) in the cap shale. This paper addresses the effects of the intrinsic anisotropy of the shales and also the existence of NFs on the Maximum Operating Pressure (MOP) in SAGD projects.

In this study, a new constitutive model is developed and incorporated to consider the effect of NFs and intrinsic anisotropy in the cap shale. A coupled numerical tool was utilized to determine the MOP for different case scenarios in the number of fracture sets, fracture density and dip angle, as well as the height. Results of all cases were analyzed to evaluate their effect on the MOP.

Results of the coupled model indicate continued integrity of the caprock for the case study project for the current operational program for almost all the considered case scenarios, except for an extreme case. Therefore, higher injection pressures than the current pressure were investigated to assess the MOP. Results indicate that the MOP was highly sensitive to the fracture density, direction, and height. Results also display a minor impact for the horizontal fractures on the MOP for the case study while fractures with the dip angle between 25° to 65° show a significant impact on the caprock integrity, hence, the MOP. Moreover, results indicate an overestimation of the MOP by up to 23% when neglecting the NFs. Comparing the results of different case scenarios with those of conventional isotropic models highlights the requirement to include the effect of NFs in caprock integrity studies.

Keywords: SAGD, Maximum Operation Pressure (MOP), Natural fractures, Shale, Caprock integrity, Anisotropy, Coupled numerical modeling

1. Introduction

Having a sealing caprock in SAGD operations is of prime importance. Steam injection expands reservoir sand, and decreases horizontal stress while increasing shear stress in the caprock, which increase the likelihood of caprock breach (Rahmati et al., 2014, 2015).

Natural Fractures (NFs) have been observed in SAGD caprocks in Alberta (Chou, 2014). They act as potential failure planes that could be triggered when the shear stress in those planes exceeds the threshold. Natural fractures also influence the caprock response by inducing structural anisotropy in the caprock.

Another type of anisotropy, which is called intrinsic anisotropy, has been observed in shales (Donath, 1964; Hoek, 1964; McLamore and Gray, 1967; Horino and Ellickson, 1970; Ramamurthy, 1993; Karakul et al., 2010). Shales exhibit strong intrinsic anisotropy due to the existence of bedding planes and the platelet shape of shale grains. This anisotropy manifests itself in directional dependency of deformation and strength properties (Duveau, 2001). Effect of

the intrinsic anisotropy on caprock integrity for SAGD projects was addressed by Rahmati et al. (2017).

Several researchers have studied caprock integrity in SAGD projects assuming isotropic elasto-plastic behavior for the caprock and neglecting the effect of NFs and discontinuities in caprock layers (Smith, 1997; McLellan and Gillen, 2000; Collins, 2007; Chalaturnyk, 2011; Khan et al., 2011; Rahmati et al., 2013). Neglecting intrinsic and structural anisotropy seems to have a significant overestimation of the Maximum Operating Pressure (MOP). Rahmati et al. (2017) studied the effect of intrinsic anisotropy of cap shale on caprock integrity. They concluded that neglecting intrinsic anisotropy alone for a case study overestimated the MOP by 7%. They did not include enough physics to incorporate NFs in the caprock integrity assessment.

Introduced numerical model here considers both the intrinsic anisotropy and NFs for caprock shale. A coupled hydro-thermo-mechanical model was developed to assess the MOP considering both intrinsic anisotropy and NFs. The effect of NFs was incorporated by developing and implementing a new constitutive relation for shales.

The coupled tool was used in conjunction with the new constitutive model for a case study based on the public published data for MacKay River SAGD project (Suncor Energy, 2009). Suncor Energy (2013) performed a fracture characterization study in the area of interest. They reported the existence of fractures in the cap shale. However, the possible effect of NFs on the MOP is yet to be addressed.

In this study, different case scenarios in terms of fracture density, dip angle, and height were simulated to investigate their effect on the MOP in SAGD projects. Comparing the result of different case scenarios with those of conventional isotropic models highlights the need to include the intrinsic and structural anisotropy of the cap shale in caprock integrity studies.

2. Definitions

Fractures were characterized by the number of fracture sets, fracture density, dip direction and angle, height, and length. A fracture set consists of a set of parallel systematic fractures. Fracture density is considered as the number of fractures of a particular set per unit length measured in a direction perpendicular to the fracture plane (Singhal et al., 2010). Dip direction is defined as the direction of the horizontal trace of the line of the dip, measured clockwise from north (Wyllie et al., 2004). Fracture's dip angle is defined as the deviation of the fracture plane from the horizontal plane. Fracture spacing describes the average perpendicular distance between two adjacent fractures of the same set and is equal to the inverse of fracture density. Fracture height is the trace extent of the fractures in a sampling area normal to the fracture length (see Figure 1). Fracture length is a measure of the extent of development of fracture surface (Singhal et al., 2010).

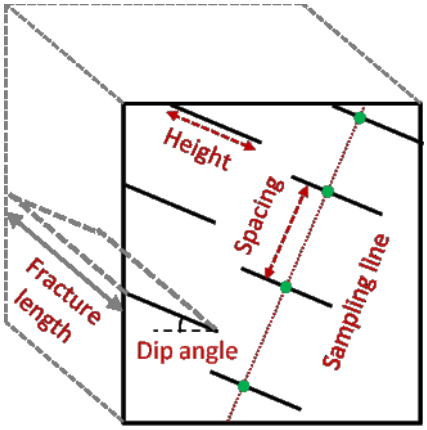

Figure 1 Definition of the attributes of natural fractures

3. Theoretical Background of the Constitutive Model

In most cases, the caprock of a petroleum reservoir consists of shale. Different researchers have demonstrated that the elastic and plastic properties of shale are highly anisotropic (McLamore and Gray, 1967; Sone, 2012). In the elastic range, stratification of shales leads to transverse isotropy which can be incorporated in the Hookes' law (Hemsing, 2007; Puzrin, 2012):

$$\begin{Bmatrix} e^e_{xx} \\ e^e_{yy} \\ e^e_{zz} \\ e^e_{xy} \end{Bmatrix} = \begin{bmatrix} 1/E_h & -\upsilon_{vh}/E_v & -\upsilon_{hh}/E_h & 0 \\ -\upsilon_{hv}/E_h & 1/E_v & -\upsilon_{hv}/E_h & 0 \\ -\upsilon_{hh}/E_h & -\upsilon_{vh}/E_v & 1/E_h & 0 \\ 0 & 0 & 0 & 1/2G_{hv} \end{bmatrix} \begin{bmatrix} \sigma_{xx} \\ \sigma_{yy} \\ \sigma_{zz} \\ \sigma_{xy} \end{bmatrix} \quad (1)$$

where σ and ε are the second-order stress and strain tensors, respectively; E_h and E_v are the Young moduli in the horizontal and vertical directions, respectively; G_{hv} is the cross-shear modulus between a plane of isotropy and the perpendicular plane; υ_{ab} is the Poisson's ratio, where "a" and "b" indicate the stress direction and the direction of the strain component caused by this stress (vertical v or horizontal h), respectively. It should be mentioned that x and z indices are in horizontal directions and y is in vertical direction.

McLamore and Gray (1967) proposed a variable cohesion and friction angle theory to capture the anisotropic behavior of shale in the plastic range. They proposed the following equations for shale's strength properties:

$$c(\theta) = A_{1,2} - B_{1,2}cos\left(2\left(\theta_{min,c} - \theta\right)\right)^n \quad (2)$$

$$\varphi(\theta) = arctan\left(C_{1,2} - D_{1,2}cos\left(2\left(\theta_{min,\varphi} - \theta\right)\right)^m\right) \quad (3)$$

where θ is the angle between the maximum principal stress and the bedding plane direction; $c(\theta)$ and $\varphi(\theta)$ are cohesion and friction angle, respectively; $\theta_{min,c}$ and $\theta_{min,\varphi}$ are the value of θ corresponding to the minimum cohesion and friction angle, respectively; A_1, B_1 and C_1, D_1 are

constants that describe the variance over the range of $0^{\circ} \leq \theta \leq \theta_{min,c}$ and $0^{\circ} \leq \theta \leq \theta_{min,\varphi}$, respectively; A_2, B_2 and C_2, D_2 are constants that describe the variance over the range of $\theta_{min,c} < \theta \leq 90^{\circ}$ and $\theta_{min,\varphi} < \theta \leq 90^{\circ}$, respectively; n and m are "anisotropy type" factors (McLamore and Gray, 1967).

A ubiquitous joints model theory proposed by Clark (2006) was adopted to incorporate the effect of NFs in the model. . The ubiquitous joints model represents a set of fractures that are triggered when their yield criterion is satisfied. The ubiquitous joints model was combined with the elastic transverse anisotropy and the variable cohesion-friction model proposed by McLamore and Gray (1967) to come up with an anisotropic model which accounts for both intrinsic and structureal anisotropy. In the proposed model, yielding may occur either in the solid or along the fractures, or both, depending on the stress state, fracture's direction, and strength properties of the solid and fractures.

In this constitutive model, the plastic deformation is first calculated due to matrix yield. The new stresses are then analyzed and updated for the fracture yield. Mohr-Coulomb criterion was used for the fracture yield detection in the ubiquitous joints model:

$$\tau = -\sigma_n tan\varphi_f + c_f \tag{4}$$

where τ and σ_n are the shear stress and effective normal stress on the fracture plane, respectively; φ_f is the fracture friction angle; and c_f is the fracture cohesive strength. For the sign convention, compressive stress is assumed to be negative.

Figure 2 illustrates the global $(x\ y)$ and local $(\acute{x}\ \acute{y})$ coordinate frames for the presentation of NFs. Angle ξ denotes the angle between the fracture plane and the global horizontal coordinate. If ξ is less than or equal to 90°, it is equal to the dip angle. If ξ is greater than 90°, it is equal to the sum of dip angle and 90°.

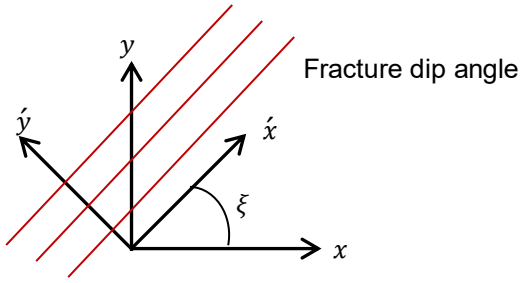

Figure 2 A fracture set with the dip angle of ξ with respect to the x axis of the global reference frame

The global and local stress components are denoted as σ_{ij} and $\acute{\sigma_{ij}}$, respectively. These global stresses are resolved into local components by stress transformation (Fjaer et al., 2008):

$$\begin{bmatrix} \acute{\sigma_{xx}} \\ \acute{\sigma_{yy}} \\ \acute{\sigma_{zz}} \\ \acute{\tau} = \acute{\sigma_{xy}} \end{bmatrix} = R \begin{bmatrix} \sigma_{xx} \\ \sigma_{yy} \\ \sigma_{zz} \\ \sigma_{xy} \end{bmatrix} \tag{5}$$

where rotational matrix $[R]$ is as follows:

$$R = \begin{bmatrix} cos\,\xi^2 & sin\,\xi^2 & 0 & 2\,sin\,\xi\,cos\,\xi \\ sin\,\xi^2 & cos\,\xi^2 & 0 & -2\,sin\,\xi\,cos\,\xi \\ 0 & 0 & 1 & 0 \\ -\,sin\,\xi\,cos\,\xi & sin\,\xi\,cos\,\xi & 0 & cos\,\xi^2 - sin\,\xi^2 \end{bmatrix} \quad (6)$$

With this notation, the local expression of incremental elastic stress has the form:

$$\begin{bmatrix} \Delta\sigma'_{xx} \\ \Delta\sigma'_{yy} \\ \Delta\sigma'_{zz} \\ \Delta\acute{t} \end{bmatrix} = [\acute{K}] \begin{bmatrix} \Delta e'^{\,e}_{xx} \\ \Delta e'^{\,e}_{yy} \\ \Delta e'^{\,e}_{zz} \\ \Delta e'^{\,e}_{xy} \end{bmatrix} \quad (7)$$

in which

$$[\acute{K}] = [R][K][R]^{-1} \quad (8)$$

where matrix $[K]$ is the stiffness matrix, and e'_{ij} is the strain in the local coordinate system, and the superscript "*e*" stands for "elastic".

Yield criteria may be presented in the $(\sigma'_{yy}, \acute{t})$ plane, as illustrated in Figure 3:

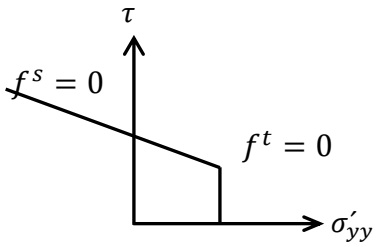

Figure 3 Fracture's yield criterion

Mohr-Coulomb criterion is used as the shear yield envelope for the NF:

$$f^S = -\acute{t} - \sigma'_{yy} tan\varphi_f + c_f \quad (9)$$

And the tensile yield criterion for the NF is defined by:

$$f^t = \sigma_f^t - \sigma'_{yy} \quad (10)$$

where σ_f^t is the tensile limit of the fractures.

The shear and tensile potential functions (g^S, and g^t) correspond to non-associated flow rules with dilatancy, ψ_f, as follows:

$$g^S = -\acute{t} - \sigma'_{yy}\,tan\,\psi_f \quad (11)$$

$$g^t = -\sigma'_{yy} \quad (12)$$

Non-associated flow rule for the shear and tensile yield are defined as follows (Fjar et al., 2008):

$$\Delta e_{ij}^P = \lambda_S \frac{\partial g^s}{\partial \sigma_{ij}} \quad (13)$$

$$\Delta e_{ij}^P = \lambda_t \frac{\partial g^t}{\partial \sigma_{ij}} \quad (14)$$

where λ_S and λ_t are the constants of proportionality for shear and tensile yield modes, respectively, and superscript "p" stands for "plastic".

Combining Eq. (11) and Eq. (13), plastic strain increments due to the shear yield along the fracture are expressed as follows:

$$\begin{bmatrix} \Delta e'_{xx}{}^{P} \\ \Delta e'_{yy}{}^{P} \\ \Delta e'_{zz}{}^{P} \\ \Delta e'_{xy}{}^{P} \end{bmatrix} = \begin{bmatrix} 0 \\ -\lambda_S \tan\psi_f \\ 0 \\ -\lambda_S \end{bmatrix} \tag{15}$$

Plastic strain increments due to tensile yielding can be obtained by combining Eq. (12) and (14):

$$\begin{bmatrix} \Delta e'_{xx}{}^{P} \\ \Delta e'_{yy}{}^{P} \\ \Delta e'_{zz}{}^{P} \\ \Delta e'_{xy}{}^{P} \end{bmatrix} = \begin{bmatrix} 0 \\ -\lambda_t \\ 0 \\ 0 \end{bmatrix} \tag{16}$$

Elastic strain increments are obtained by subtracting the plastic strain increments from the total strain increments. Assuming that the plastic contributions of intact rock and NFs are additive, the elastic guesses in Eq. (7) are the stresses here, obtained after the application of plastic corrections related to the yielding of intact material. Using this approach, it may be shown that the new stress state in the case of shear and tensile yield may be expressed as follows, respectively.

$$\begin{bmatrix} \acute{\sigma}^N_{xx} \\ \acute{\sigma}^N_{yy} \\ \acute{\sigma}^N_{zz} \\ \acute{\tau}^N \end{bmatrix} = \begin{bmatrix} \sigma'_{xx} \\ \sigma'_{yy} \\ \sigma'_{zz} \\ \acute{\tau} \end{bmatrix} + \begin{bmatrix} \acute{K}(1,2)\tan\psi_f\,\lambda_S + \acute{K}(1,4)\lambda_S \\ \acute{K}(2,2)\tan\psi_f\,\lambda_S + \acute{K}(2,4)\lambda_S \\ \acute{K}(3,2)\tan\psi_f\,\lambda_S + \acute{K}(3,4)\lambda_S \\ \acute{K}(4,2)\tan\psi_f\,\lambda_S + \acute{K}(4,4)\lambda_S \end{bmatrix} \tag{17}$$

$$\begin{bmatrix} \acute{\sigma}^N_{xx} \\ \acute{\sigma}^N_{yy} \\ \acute{\sigma}^N_{zz} \\ \acute{\tau}^N \end{bmatrix} = \begin{bmatrix} \sigma'_{xx} \\ \sigma'_{yy} \\ \sigma'_{zz} \\ \acute{\tau} \end{bmatrix} + \begin{bmatrix} \acute{K}(1,2)\lambda_t \\ \acute{K}(2,2)\lambda_t \\ \acute{K}(3,2)\lambda_t \\ \acute{K}(4,2)\lambda_t \end{bmatrix} \tag{18}$$

where superscript "N" stands "new stress state", and $\acute{K}(i,j)$ is the component of stiffness matrix.

Considering that the new stresses should lie on the shear yield envelope, shear constant of proportionality may be calculated by combining Eq. (6) and Eq. (17), and expressed as follows:

$$\lambda_S = \frac{f^s\left(\sigma'_{yy}, \tau\right)}{\left(\acute{K}(4,2)\tan\psi_f + \acute{K}(4,4) + \acute{K}(2,2)\tan\psi_f\tan\varphi_f + \acute{K}(2,4)\tan\varphi_f\right)} \tag{19}$$

Using the same reasoning as described above, tensile constant of proportionality may be calculated by combining Eq. (10) and Eq. (18), and expressed as:

$$\lambda_t = \frac{f^t\left(\sigma'_{yy}\right)}{\acute{K}(2,2)} \tag{20}$$

Finally, after calculating the new stresses in the local coordinate system, the stresses resolve back

into the global coordinate system by using Eq. (5).

Presented formulation is adequate to consider the effect of a single fracture set. To consider the effect of multiple fracture sets, one yield criterion for each single fracture set is added. The proposed constitutive law can consider shale intrinsic anisotropy in elastic and plastic ranges. In addition, it can consider the effect of multiple fracture sets in the caprock. The criterion was imbedded in FLAC software (ICG, 2011) for the caprock integrity analysis and the MOP assessment in SAGD projects.

4. Numerical Model

Two commercial finite difference software packages (FLAC, a geomechanical software package developed by ITASCA (Itasca Consulting Group, 2011) and STARS, a flow simulator developed by CMG (CMG, 2013) were linked to perform the simulations. A MATLAB code was used as an interface to run the modules and also update the shared parameters. Sequential coupling approach with a convergence tolerance of 5% was used to link the fluid-flow module with the Geomechanics module. Figure 4 shows a schematic of the coupling approach. Further details on the coupling approach could be found in Rahmati et al. (2017).

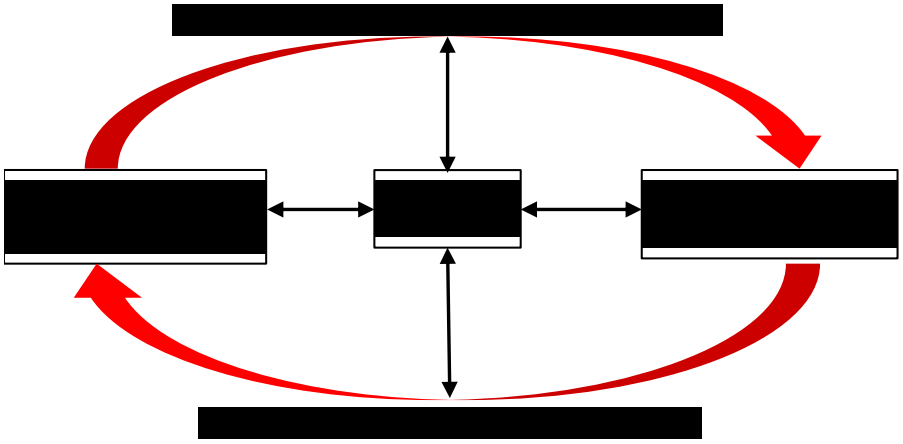

Figure 4 Sequential coupling scheme (after Rahmati et al., 2014)

5. Case Study

This section demonstrates the importance of including cap shale's intrinsic anisotropy and NFs in caprock integrity studies by presenting the results of a case study.

5.1. Input Data

Public data related to Pad C MacKay River SAGD project were used for this study to ensure consistent data. Some input data were assumed as they were not publicly available. Thus, this work should not be regarded as caprock integrity investigation for this particular project. It should only be regarded as an effort to understand the impact of NFs and intrinsic anisotropy of cap shale on the MOP in SAGD projects.

Except for the characteristics of the natural fractures, the input data for this study can be found in Rahmati et al. (2017). The data consist of in-situ stresses, hydraulic, thermal, and mechanical

properties, and anisotropic mechanical properties.

The rest of this section presents the geological information and the assumed strength parameters for the NFs.

5.1.1. *Geological Description of Natural Fractures*

Suncor Energy (2013) reported the existence of NFs in Clearwater formation and Wabiskaw member in MacKay River SAGD project. They indicated that there was no mineralization or bitumen staining in fractures in the wells examined to date. They observed higher fracture density for the lower part of Clearwater Shale and Wabiskaw A shale than for the Wabiskaw D mudstone. They also observed that Wabiskaw A shale was the most fractured unit (2.6 frac./m), followed by Clearwater formation (2.4 frac./m). Wabiskaw-D Mudstone is the least fractured unit (0.2 frac./m). The geological evidence for the existence of NFs warrants the consideration of NFs in the caprock integrity analysis.

Information about the dip angle and dip direction of NFs in Wabiskaw member and Clearwater shale were not publicly available. Hence, this work assumes the fracture geometry and properties in a sensitivity analysis. These assumptions are not representative of the actual fractures for this particular site. The analysis is solely to show how the existence of NFs can impact the MOP level. In this study, a uniform fracture distribution was assumed. Further, a linear fracture density of 2.5 frac./m was considered for the base case for both Clearwater and Wabiskaw shales. The fractures were assumed to be systematic (not random) with NE-SW direction (dip direction of 315°) (parallel to the SAGD wells) with 40-50° dip angle.

5.1.2. *Strength Properties of Ubiquitous Fractures*

A critical issue for this study was to determine the strength parameters of ubiquitous fractures. A series of hypothetical numerical direct shear tests were performed with FLAC to calculate the strength properties of elements containing fractures (Figure 5). The main purpose of this hypothetical numerical model was to smear the NF effect to the entire medium as the fracture size is relatively small in comparison with the size of numerical grid blocks. The results of numerical direct shear test were verified against analytical solutions proposed by Wittke (1990).

The sample size for direct shear test was selected to be 4 m by 4 m (Figure 5) based on the Representative Elementary Volume (REV) assessment for these fractures. The REV is the smallest volume over which a measurement can be made that will yield a value representative of the whole (Hill, 1963). Different fracture densities (1.75 to 8.5 frac./m) were considered to evaluate the strength properties of the rock mass (Figure 5). Fractures were uniformly distributed throughout the solid inFigure 5. Niven and Duestch (2010) asserted that conventional random fracture distribution, which is commonly used for Discrete Fracture Networks (DFNs), does not represent realistic fracture distribution (Niven et al., 2010). They studied two NF maps for outcrop rocks in Northern Alberta and Vernazza, Italy. They concluded that for both examples, NFs were not distributed randomly; rather they were created according to in situ stress directions and magnitudes. Thus, random distribution of NFs is rare when tectonic forces created them (Niven and Duestch, 2010). However, other sources of development of NFs (e.g., Glacio-tectonic disturbance, Gravity slumping, and Diagenetic mineral conversion) have also been observed in Alberta (Tsui et al., 1988; Gregor, 1997; Ding et al., 2012). The authors assumed uniform distribution with equal fracture spacing (see Figure 5). In Figure 5, fractures are shown as black

lines.

The strength parameters for Clearwater/Wabiskaw shale were assumed to be the same as the assigned parameters by Rahmati et al. (2017) for same layers. As most of the fractures for the studied area have no infill materials (Suncor Energy, 2013), cohesion and tensile strength were assumed to be zero for the NFs. The friction angle of NFs was assumed to be 15°. The authors are not aware if experimental measurements have been conducted for this property for Clearwater and Wabiskaw shales particularly for this site.

Equivalent cohesion and friction angle for different fracture densities were calculated based on the results of numerical direct shear tests for both Wabiskaw and Clearwater shale. Figure 6shows the equivalent friction angle and cohesion for different fracture densities.

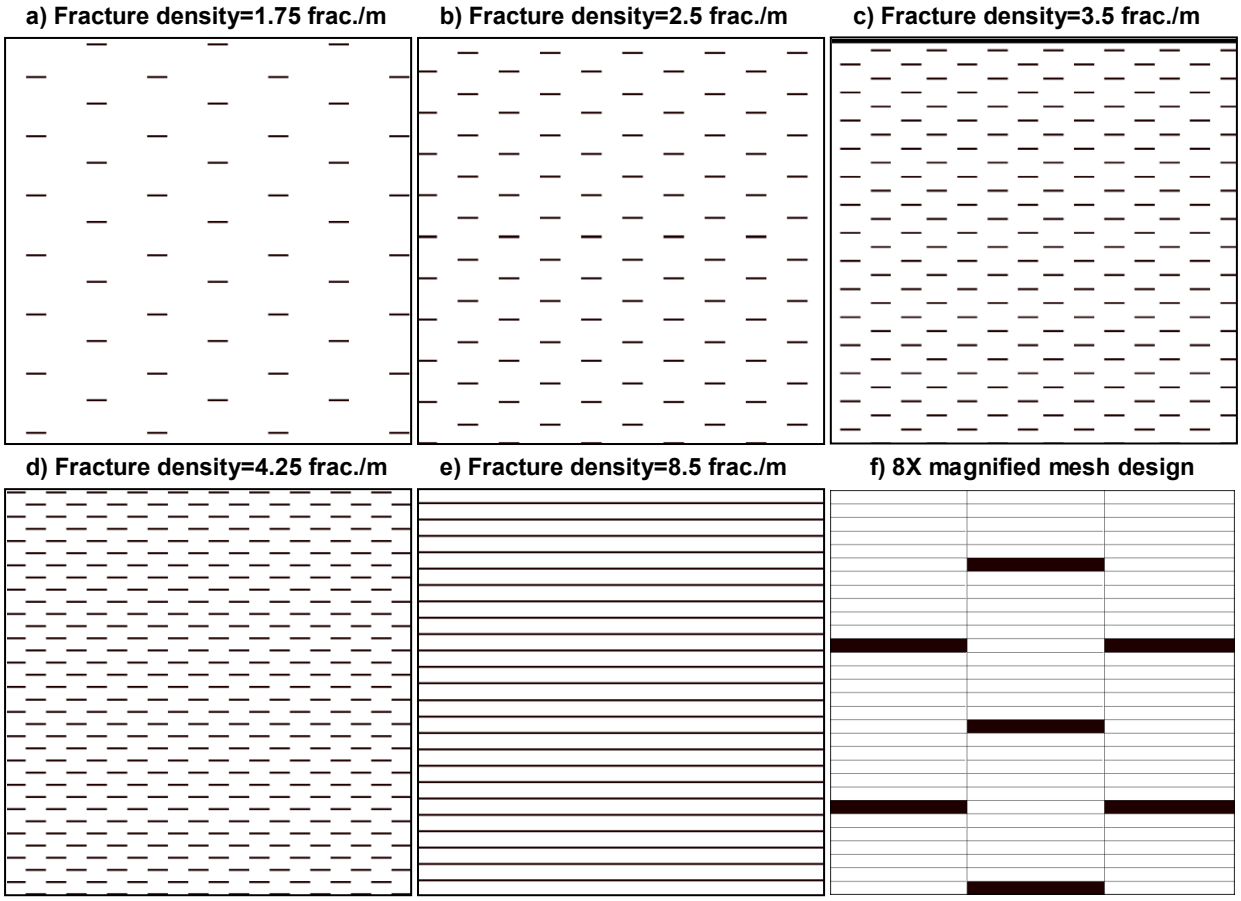

Figure 5 (a-e) Schematic of assumed NF distribution for different fracture densities and (f) magnified mesh design

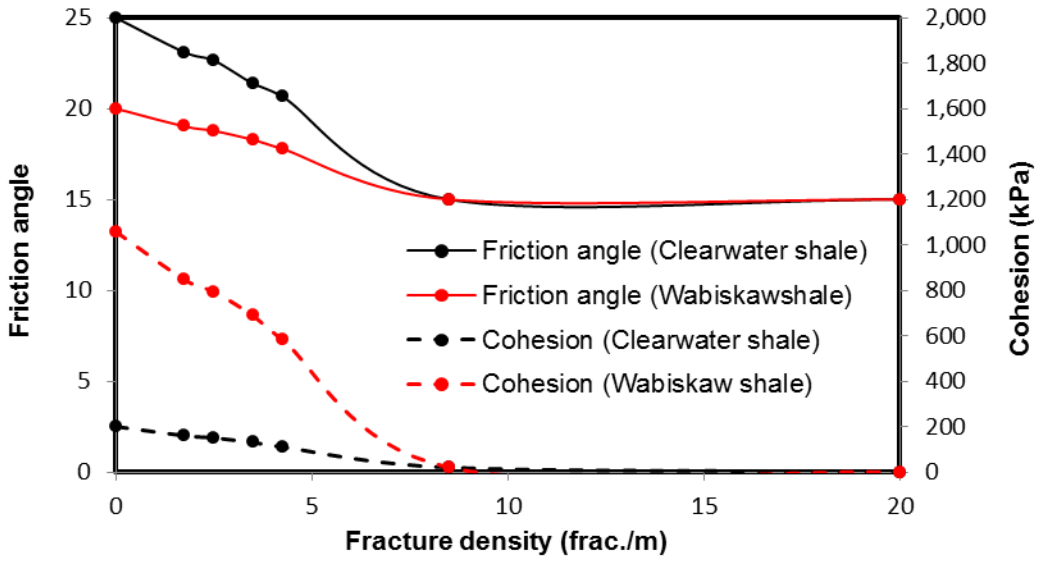

Figure 6 Equivalent friction angle and cohesion for different fracture densities in Clearwater and Wabiskaw shales

5.1.3. *Effect of Fracture Attributes on Strength Properties of Ubiquitous Fractures*

Because a comprehensive fracture characterization has not been published for the case study area, a parametric study by varying the number of fracture sets was performed, fracture density, and fracture height and dip angle to investigate their effect on the MOP (Table 1). Non-fractured model with the assumption of isotropic rock was considered as the base case. To study the effect of fracture density on the MOP, two cases were tested with the fracture density of 2.5 (base case) and 3.5 frac./m.

Table 1 Simulation matrix to investigate the effect of NFs on MOP

Category	Number of simulations	Fracture density (frac./m)	Fracture dip angle (ξ)	Fracture height (cm)	Number of fracture sets
[1]Non-fractured cases (isotropic and intrinsically anisotropic model)	2	--	--	--	0
Fracture density	5	2.5 and 3.5	[2]0°, 45° and 90°	20	1
Fracture dip angles	5	2.5 and 3.5	[2]0°, 45° and 90°	20	1
Fracture height	2	2.5	45° for single set/25°,45° and 65° for 3 sets	20 and 100	3
Fracture interaction	2	2.5	45° for single set/25°,45° and 65° for 3 sets	20	1 and 3

[1]Non-fractured cases do not include fracture sets. Isotropic and intrinsically anisotropic models are considered for caprock layers. Isotropic model is considered as base case.
[2]The case of 0° dip angle for fractures was not run for the density of 3.5 frac./m, as the case with the density of 2.5 frac./m showed that fractures with such dip angle have no contribution to failure.

5.2. Model Geometry, Operational Conditions, and Boundary Conditions

Five years of injection-production operation of Pad C is simulated in this paper. Steam quality, temperature, and pressure were considered to be 95%, 200 °C and 1,650 kPa, respectively (Suncor Energy, 2009).

2-D plane strain condition was assumed, which seems to be valid because of the relatively long horizontal wells compared with the distance between the wells and also, a uniform temperature distribution along the producers (Suncor Energy, 2013), which is an indication of uniform steam injection and production along the wells.

Pad C consists of six well pairs, called C1-C6. In this research, geometry and operation symmetry were assumed between C1-C3 well pairs and C4-C6 well pairs. Therefore, as shown in Figure 7, only C4-C6 well pairs were simulated. The model sides were fixed in the horizontal direction and the bottom boundary was fixed in horizontal and vertical directions.

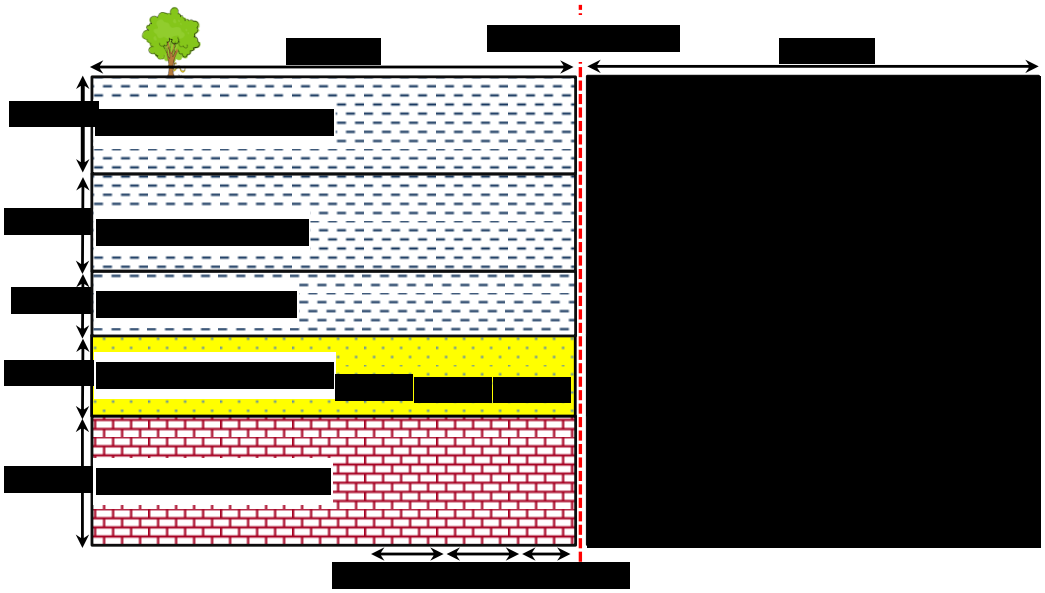

Figure 7 Model geometry (after Rahmati et al., 2017)

Numerical mesh design for the geomechanical module is presented in Figure 8. Different element sizes were used to decrease the computation time while keeping the accuracy on the sensitive layers. Figure 9 shows the fluid-flow simulator mesh design. A uniform element size was used in the fluid-flow simulator.

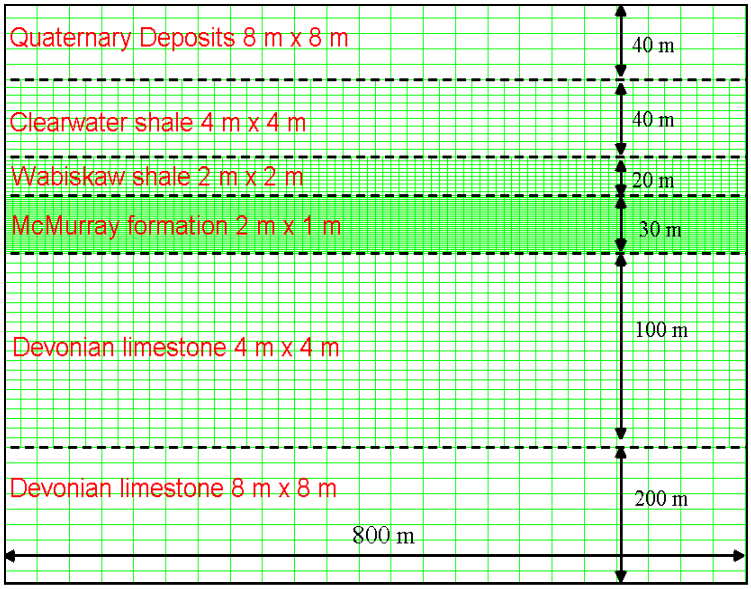

Figure 8 Geomechanical grid-block size for each layer (after Rahmati et al., 2017)

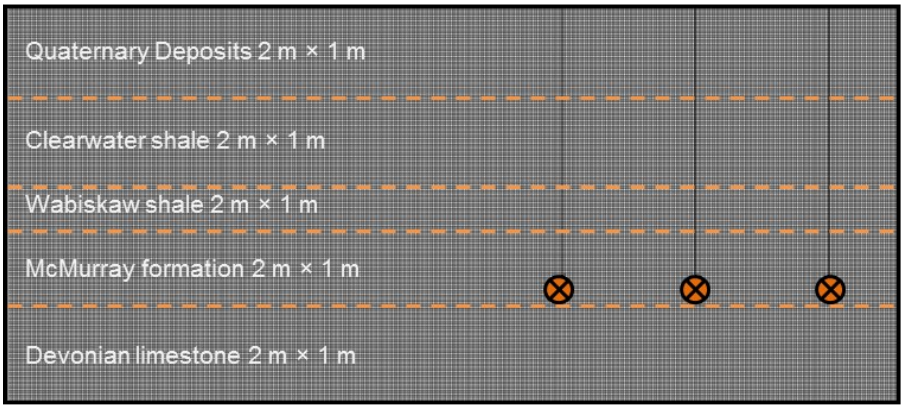

Figure 9 Numerical mesh for fluid flow for each geological layer (after Rahmati et al., 2017)

6. Results of Coupled Hydro-thermo-mechanical Model

This section considers the anisotropic non-fractured model as the base case model. For all cases, the actual well operation was applied for the first five years. At the end of five years of operations, if field injection pressures did not compromise the caprock, the injection pressures were increased beyond the actual levels to find the caprock breach pressure. The injection pressure was increased in steps, where the pressure in each step was higher than the previous by 10% of the injection pressure in the previous step. The pressure in each step was kept constant for six months.

Injection pressures were increased until the caprock breach, which was defined as the yielded zone extending from the bottom to the top of the caprock. To obtain a more accurate prediction of failure pressure, after the occurrence of caprock breach, the numerical model for the last increment was repeated at 5% and 2.5% steps rendering failure pressure with accuracy higher than 40 kPa.

6.1. Simulation Cases

The effect of four parameters (including fracture density, dip angle, height, and interaction between different fracture sets) was considered to investigate the possible effect of NFs on the MOP. Results are compared with those of anisotropic non-fractured model, which was considered as the base case.

6.1.1. *Fracture Density and Dip Angle*

Figure 10shows the yielded zone for the case with horizontal NFs ($\xi = 0°$) and fracture density of 2.5 frac./m. Failure pressure was found to be 2,392 kPa, which is the same as that of the model that considered only intrinsic anisotropy (no NFs). Figure 10 shows that the caprock failure is due to yielding in the rock matrix.

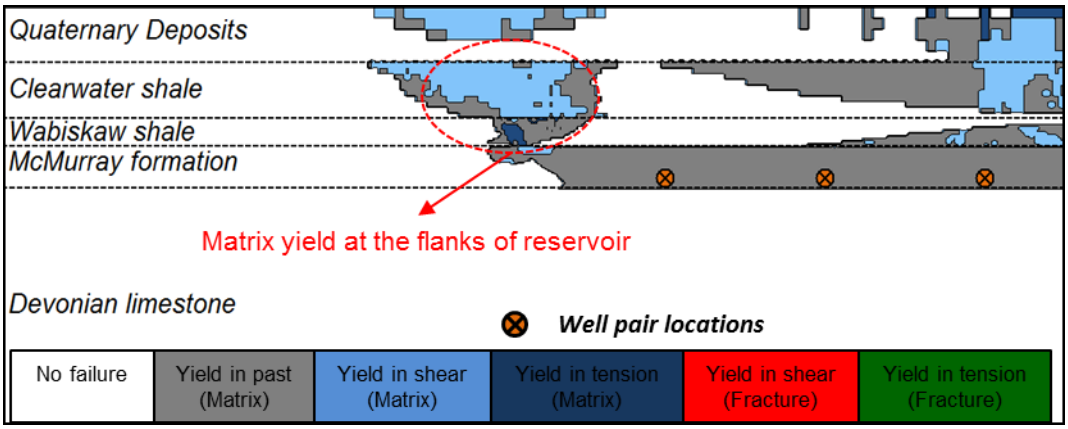

Figure 10 Yielded zones for fracture density=2.5 $frac./m$ and fracture dip angle=0°

Figure 11 displays the yielded zones for oblique fractures ($\xi = 45°$) and fracture density of 2.5 frac./m. Results show that the Clearwater shale is in shear yield due to the NFs. In this case study, failure pressure dropped from 2, 392 kPa with no NFs to 2, 145 kPa for the case with the NFs. The NFs for this case decrease the failure pressure by 11%, which indicates that the oblique fractures ($\xi = 45°$) have significant effect on failure pressure of the injector wells.

Figure 12 shows the yielded zone for vertical fractures ($\xi = 90°$) and fracture density of 2.5 frac./m. The figure shows that there is a small zone with yielded fracture at the bottom of Clearwater shale and the rest of the caprock failed due to shear matrix yield. The assumption of no additional hydraulic conductivity for the fractures compared to the matrix could be the main reason that the vertical fractures showed minor effect on caprock failure pressure. Another reason could be due the fact that the NFs growth was not considered in this study. Failure pressure in this case was found to be 2,351 kPa. The failure pressure for this case is only 1.5% less than the case without considering NFs.

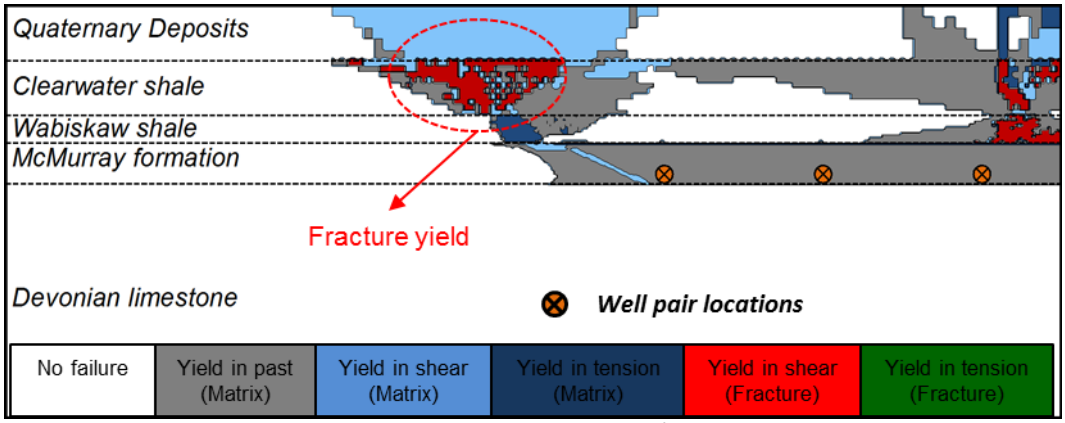

Figure 11 Yielded zones for fracture density=2.5 $frac./m$ and fracture dip angle=45°

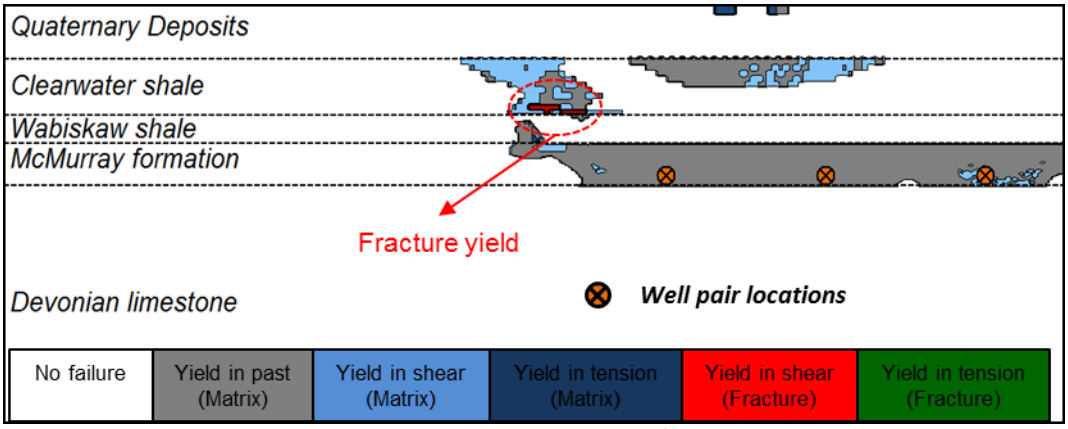

Figure 12 Yielded zones for fracture density=2.5 $frac./m$ and fracture dip angle=90°

Figure 13 presents the yielded zone for the case of fracture density of 3.5 frac./m and oblique fractures (ξ = 45°). Results show that most of the Clearwater shale, which is the main caprock in this project, was breached due to fracture yield. Failure pressure in this case was significantly lower at 1,980 kPa. The figure shows the development of a pervasive flow path network due to the NFs yield in the full thickness of the Clearwater shale. The comparison of failure pressure for this case (fracture density of 3.5 frac./m and ξ = 45°) and the case with the fracture density of 2.5 frac./m and the same fracture dip angle indicates the significant impact of fracture density on the failure pressure. Increasing the fracture density in this case from 2.5 to 3.5 frac./m decreased the failure pressure by 8%.

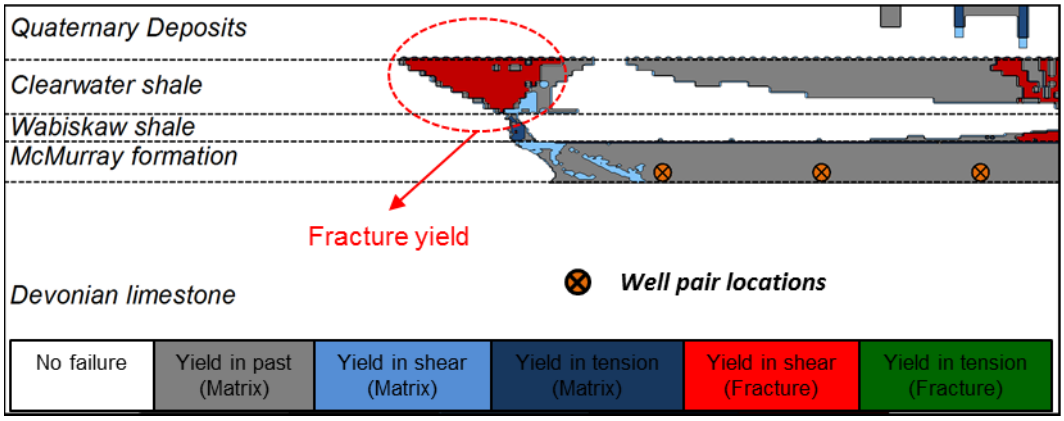

Figure 13 Yielded zones for fracture density=3.5 $frac./m$ and fracture dip angle=45°

Figure 14 illustrates the yielded zones for the case of vertical fractures, (ξ = 90°) and fracture density of 3.5 frac./m. This figure shows a yielded zone due to the NFs. Failure pressure for this case was found to be 2,310 kPa, which is close to the failure pressure for the case with vertical fractures and fracture density of 2.5 frac./m (failure pressure = 2,351 kPa). Results show that the fracture density has a minor effect on the failure pressure of vertical fractures for this case study. In this case, failure pressure was decreased by only 1% in response to 40% increase in fracture density. Also, results indicate a minor influence of vertical fractures on caprock integrity for the range of fracture density considered here. Vertical fractures could have a significant effect on caprock integrity if (1) the in situ horizontal stress is the minimum principal stress (versus the study case in which vertical stress is the minimum principal stress, and (2) they possess high hydraulic conductivity that can lead to hydraulic fracturing.

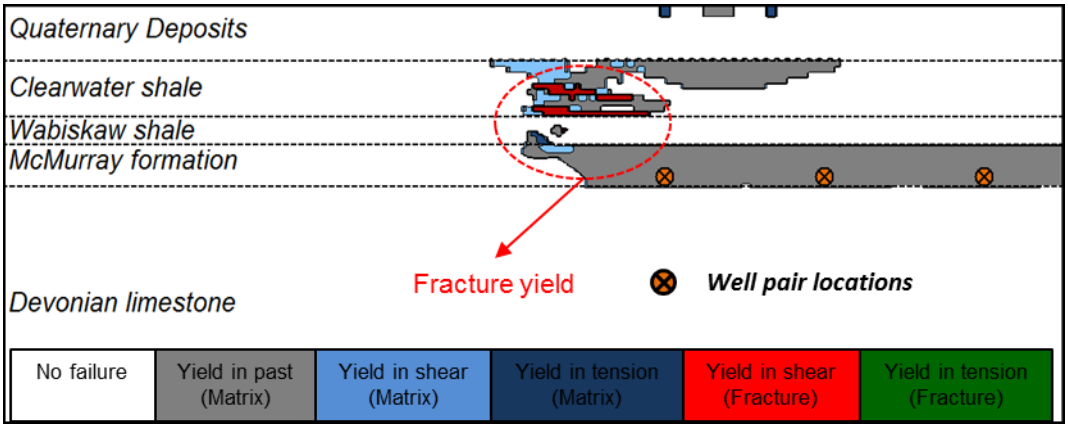

Figure 14 Yielded zones for fracture density=3.5 $frac./m$ and fracture dip angle=90°

6.1.2. *Interaction between Different Fracture Sets*

Results shown before were only with the consideration of one set of fractures. To investigate the possible interaction of different fracture sets, a case was considered with three fracture sets with 25°, 45° and 65° dip angles. Fracture height and total density were kept at 20 cm and 2.5 frac./m for all fracture sets combined. Fracture density for fracture sets with dip angles of 25°, 45°, and 65° were assumed to be 0.5,1, and 1 frac./m. Therefore, the total fracture density in different dip angles was equal to 2.5 frac./m.

Results show caprock breach at 2,227 kPa, which is higher than the failure pressure for single fracture set with 45° dip angle (2,145 kPa). Failure pressure in this case is 3.6% higher than the case with 45° dip angle considering only one set of NFs with the same fracture density. This is because, for this case study, the NFs with 45° dip angle are more prone to failure than 25° or 65° NFs. Figure 15 shows the yielded zones for the case with three fracture sets. Yielded fractures are seen to have conical shape with more spread at shallower depth, due likely to smaller normal stresses on NF planes at shallower depth. The yielded zone in this case shows a network of yielded NFs and it could be a potential flow path for injected fluid and bitumen through the caprock.

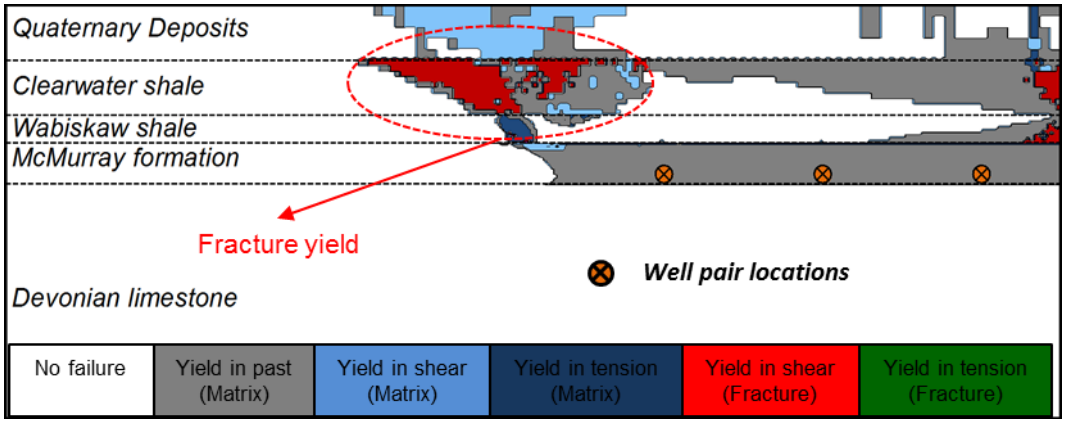

Figure 15 Yielded zones for three sets of the fractures with 25°, 45° and 65° dip angle of fracture density=2.5 $frac./m$ and fracture height=20 cm

6.1.3. *Fracture Height*

Fracture height was assumed to be 20 cm for all previous cases. To investigate the effect of fracture height on failure pressure, a case was considered with three sets of fractures with dip angle of 25°, 45° and 65° and fracture height of 100 cm. As expected, caprock was more prone to failure in this case due to the larger fractures. The result was caprock failure in the third year of production with the existing operating pressure (injection pressure of 1,650 kPa). Figure 16 depicts the yielded zone for this case which shows shear yielded fractures across the Clearwater shale. Figure shows yielded NFs in the Clearwater shale above the steam champers and also at the flanks. By comparing the failure pressure of this case (1,650 kPa) with the case with fracture height of 20 cm (2,227 kPa), it can be concluded that the failure pressure is highly affected by the length of NFs. Failure pressure in this case was dropped by 26% in comparison with the case with the fracture height of 20 cm. Results show the importance of accurate characterization of NFs in terms of the height and dip angle.

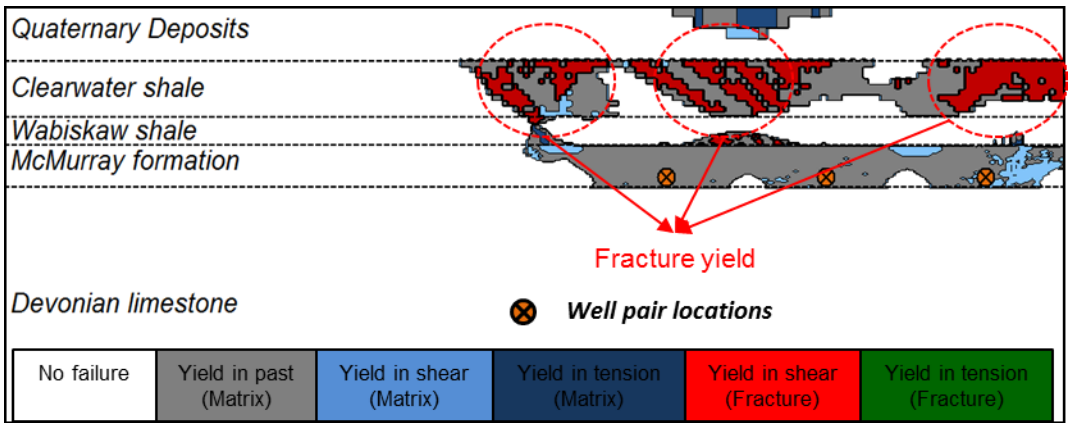

Figure 16 Yielded zones for three sets of the fractures with 25°, 45° and 65° dip angle of fracture density=2.5 $frac./m$ and fracture height=100 cm

6.2. Comparison with Models with no NFs

To highlight the effect of including NFs in the constitutive model, calculated failure pressures are compared with those of isotropic and intrinsically anisotropic models published by Rahmati et al. (2017).

Figure 17 shows the injection pressures for caprock breach for different cases. The figure

indicates the lowest failure pressure among the cases with 20 cm fracture height belongs to the case with the dip angle of 45° and fracture density of 3.5 frac./m. The highest failure pressure can be observed for the model with the assumption of isotropic material for the caprock. This figure indicates conventional isotropic models can overestimate the failure pressure. The predicted failure pressure for the case of 100 cm fracture was low as results indicated caprock failure in the 3rd year of production with the operating pressure that was exercised in the field.

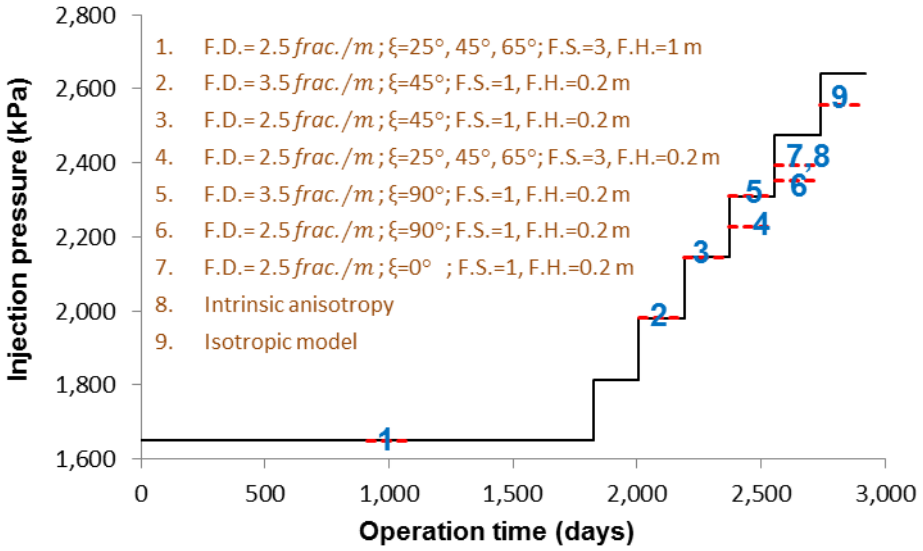

Figure 17 Injection pressures at caprock failure for Injector C6 (F.D., F.S. and F.H. stand for fracture density, number of fracture sets and fracture height, respectively)

Table 2 presents the failure pressures for different sensitivity cases in terms of injector well pressure. Failure pressures in Table 2 are affected by the assumptions in the numerical model and uncertainties for the input data. One should consider a safety factor to convert the failure pressures to MOP. The MOPs in Table 2 were calculated by applying the safety factor of 1.25 to the failure pressure. The safety factor of 1.25 is considered by the Alberta Energy Regulator (AER) for calculating MOP for shallow thermal in situ oil sands applications (AER Bulletin, 2014).

By comparing different cases in Table 2 and considering the case with isotropic caprock as the base case, it can be seen that

- Neglecting intrinsic anisotropy resulted an overestimation of the MOP by 7%;
- For the sensitivity cases attempted, neglecting structural anisotropy (i.e., NFs) led to an overestimation of the MOP by up to 35% compared with the isotropic model.
- Oblique NFs had major effect while horizontal NFs showed a negligible effect on the MOP. Vertical fractures showed some effect on the MOP (8-10% compared with the case with isotropic assumption without NFs).
- Including multiple sets of NFs (instead of assuming NFs in one dip angle) has a significant effect on the MOP of injector wells. For the specific case study of this research and the same fracture density (2.5 frac./m), MOP was increased by 3.6% when

considering three sets of NFs in comparison with the case considering NFs in dip angle of 45°.

- Fracture height has a significant effect on the MOP of injector wells. The results show that with the increase of the fracture height from 20 cm to 100 cm, MOP was dropped by 35%. Therefore, accurate characterization of NFs is essential for caprock integrity studies.
- Fracture density affects the MOP in SAGD operations. MOP is decreased by increase of fracture density. In this study, MOP was decreased by 8 % with 40% increase of fracture density for the case of oblique NFs.

Vertical fractures, if triggered, could highly enhance the possibility of vertical leakage of the steam/bitumen via NFs. The possible hydraulic contribution of NFs was not considered for this study as Suncor Energy (2013) reported that the NFs in the studied area were non-conductive.

Table 2 Injection pressures at failure for injector wells

Category		Fracture density ($frac./m$)	Fracture Height	Fracture sets	Fracture dip angle	[2]MOP	Failure pressure (kPa)	Difference with [3]isotropic model
Fracture interaction	Fracture height	2.5	100	3	ξ=25°,45° and 65°	1,320	[1]1,650	35%
		2.5	20	3	ξ=25°,45° and 65°	1,781	2,227	13%
	Fracture density and dip angle	2.5	20	1	ξ=45°	1,716	2,145	16%
		2.5	20	1	ξ=0°	1,913	2,392	7%
		2.5	20	1	ξ=90°	1,880	2,351	8%
		3.5	20	1	ξ=45°	1,584	1,980	23%
		3.5	20	1	ξ=90°	1,848	2,310	10%
	[4]Non-fractured cases	[3]Isotropic model	20	0	-	2,045	2,557	0%
		Intrinsic Anisotropy	20	0	-	1,913	2,392	7%

[1]Model failed at the third year of operation with current operating injection pressure.
[2]MOP is calculated considering 1.25 safety factor.
[3]Isotropic model is considered as the base case and other cases are compared with it.
[4]These cases were outlined by Rahmati et al. (2017).

7. Conclusion

A hydro-thermo-mechanical model was developed to find the MOP in SAGD projects

considering the intrinsic anisotropy of shales and NFs. A novel elasto-plastic constitutive model was developed for this study which takes into consideration elastic anisotropy, anisotropic strength properties, and different sets of NFs.

Numerical direct shear tests were performed on samples with different fracture densities to find the equivalent strength parameters for ubiquitous fracture sets. Results showed that with the increase of fracture density, equivalent friction angle and cohesion for the sample dropped.

A series of coupled numerical models was performed to evaluate the failure pressure for a case study considering intrinsic and structural anisotropy (NFs) of shale formations. Failure pressure was defined as the pressure that results the expansion of yielded zone from reservoir-caprock interface up to the caprock-quaternary deposits interface. A sensitivity analysis was performed for different fracture densities, heights, dip angles and number of fracture sets. The maximum operating pressure was calculated by dividing the failure pressure by the safety factor of 1.25.

Results for the case study showed that the isotropic model overestimated the MOP by 8% to 23% depending on fracture density and dip angle for the cases with 20 cm height of fracture. Results showed that the inclined fractures with the dip angle of 45° had significant effect on the MOP, where the MOP dropped by 23% and 16% for fracture density of 3.5 and 2.5 frac./m, respectively, compared to those estimated using the isotropic assumption. Vertical fractures did not show significant effect on the MOP due to the specific in situ stress pattern and negligible hydraulic conductivity of NFs in the case study. Results indicated that ignoring the structural anisotropy in caprock could potentially cause a remarkable overestimation of the MOP that could be avoided by introduced numerical assessment.

In this study, the hydraulic contribution of the NFs was neglected as published reports indicated little hydraulic conductivity for the NFs. Natural fractures could act as significant channels for fluid flow when triggered by applied stresses. The model could be improved by including the hydraulic contribution of triggered NFs.

Nomenclature

A, B, C, D = Constants in McLamore and Gray strength criterion

C_{ijkl} = Compliance tensor

c = Cohesion, kPa

E_i = Young's modulus in i direction, MPa

e_{ij} = Strains components

f = Failure criterion function

G_{hv} = Cross-shear modulus, MPa

g = Potential function

K = Stiffness matrix

m, n = Anisotropy type factors

R = Orthogonal transformation matrix

γ_P = Plastic shear strain

ε_V = Volumetric strain

θ = Angle between plane of anisotropy and maximum principal stress

λ = Constant of proportionality in non-associated flow rule

ξ = Fracture dip angle, ° σ_{lk} = Stress tensor, kPa

$\sigma_1' \; and \; \sigma_3'$ = Maximum and minimum principal effective stresses, kPa

τ = Shear stress, kPa

υ_{ab} = Poisson's ratio

φ = Friction angle, °

ψ = Dilation angle, °

ϕ = Porosity

Acknowledgment

The authors would like to acknowledge the research funding for this study provided by NSERC through CRDPJ 387606-09.

References

AER Bulletin, 2014. *Regulatory Approach for Shallow Thermal In Situ Oil Sands Applications in the Wabiskaw-McMurray Deposit of the Athabasca Oil Sands Area*. January, Retrieved from https://www.aer.ca/documents/bulletins/AER-Bulletin-2014-03.pdf.

Chalaturnyk, R.J. 2011. Observations on SAGD Caprock Integrity. In Recovery–2011 CSPG CSEG CWLS Convention.

Clark, I.H. 2006. Simulation of Rockmass Strength Using Ubiquitous Joints. In: R. Hart & P. Varona (eds), Numerical Modeling in Geomechanics-2006; Proc. 4th International FLAC Symposium, Madrid, May 2. Paper No. 08-07.

CMG, 2013. *STARS 2013.11*, User Manual.

Collins, P.M. 2007. Geomechanical Effects on the SAGD Process. *SPE Reservoir Evaluation and Engineering*. **10**(4): 367-375. SPE-97905-PA.

Ding, W., Li, C., Li, C., Xu, C., Jiu, K., Zeng, W., and Wu, L. 2012. Fracture Development in Shale and Its Relationship to Gas Accumulation. *Geoscience Frontiers*, **3**(1): 97-105.

Donath, F.A. 1964. *Strength Variation and Deformational Behavior in Anisotropic Rock*. State of the Earth in the Earth's Crust. New York: Elsevier, 281-98.

Duveau, G., Tiantang, Y., and Shao, J.F. 2001. Modelling of Anisotropy in Elastoplastic Sedimentary Rocks. In DC Rocks 2001 the 38th US Symposium on Rock Mechanics (USRMS), Washington D.C., 7-10 July. ARMA-01-1517.

Fjaer, E., Holt, R. M., Raaen, A. M., Risnes, R., et al. 2008. *Petroleum Related Rock Mechanics*, Elsevier, Amsterdam.

Gregor, V.A. 1997. Mannville Linears in the Lloydminster Heavy Oil Area and Their Relationship to Fractures and Fluid Flow in the Western Canada Sedimentary Basin. *Canadian society of Petroleum Geologists*, 428-474.

Hemsing, D.B. 2007. *Laboratory Determination of Seismic Anisotropy in Sedimentary Rock from the Western Canadian Sedimentary Basin*. MS thesis, University of Alberta, Edmonton, Canada (Fall 2007).

Hill, R. 1963. Elastic Properties of Reinforced Solids: Some Theoretical Principles. *Journal of the Mechanics and Physics of Solids*, **11**(5): 357-372.

Hoek, E. 1964. Fracture of Anisotropic Rocks. *Journal of the South African Institute of Mining and Metallurgy*, **64**(10):510–518.

Horino, F.G. and Ellickson, M.L. 1970. *A Method for Estimating Strength of Rock Containing Planes of Weakness*. Vol. 7449. US Dept. of Interior, Bureau of Mines.

Itasca Consulting Group, 2011. FLAC (Fast Lagrangian Analysis of Continua) User's Guide. 5th. 7. Itasca Consulting Group Inc, Minneapolis, Minnesota.

Jaeger, J.C., Cook, N.G., and Zimmerman, R. 2009. *Fundamentals of Rock Mechanics*. John Wiley & Sons.

Karakul, H., Ulusay, R. and Isik, N.S. 2010. Empirical Models and Numerical Analysis for Assessing Strength Anisotropy Based on Block Punch Index and Uniaxial Compression Tests. *International Journal of Rock Mechanics and Mining Sciences*, **47**(4): 657-665.

Khan, S., Han, H., Vishteh, M., and Khosravi, N. 2011. Caprock Integrity Analysis in Thermal Operations: An Integrated Geomechanics Approach. In WHOC-609 Proceedings for the 2011 World Heavy Oil Congress, Edmonton, Alberta. WHOC-11-609.

McLamore, R., and Gray, K.E. 1967. The Mechanical Behavior of Transversely Isotropic Sedimentary Rocks. *Journal of Engineering for Industry*, **89**(1): 62–73.

McLellan, P., and Gillen, K. 2000. Assessing Caprock Integrity for Steam-Assisted Gravity-Drainage Projects in Heavy-Oil Reservoirs. GEM Presentation, prepared for presentation at the (2000).

Michiel H., 2001, *Spline interpolation*, Encyclopedia of Mathematics, Springer, ISBN 978-1-55608-010-4.

Niven, R.B., and Duestch, C.V. 2010. On the Randomness of Natural Fractures. CCG Annual Report 12, 207.

Puzrin, A.M. 2012. *Constitutive Modelling in Geomechanics*. Zurich, Switzerland: Springer.

Rahmati, E., Nouri, A., Fattahpour, V., and Trivedi, J. 2017. Numerical Assessment of the Maximum Operating Pressure for SAGD Projects by Considering the Shale Intrinsic Anisotropy. *Journal of Petroleum Science and Engineering*, **148**: 10-20.

Rahmati, E., Nouri, A., Fattahpour, V., and Trivedi, J. 2015. Numerical Assessment of the Maximum Operating Pressure for Anisotropic Caprock in SAGD Projects. In SPE Heavy Oil Conference, Calgary, Alberta, 9-11 June. SPE-174509-MS.

Rahmati, E., Nouri, A., and Fattahpour, V. 2014. Caprock Integrity Analysis during a SAGD Operation Using an Anisotropic Elasto-Plastic Model. In SPE Heavy Oil Conference, Calgary, Alberta, 10-12 June. SPE-170114-MS.

Rahmati, E., Nouri, A., and Rahmati, H. 2013. Numerical Assessment of Caprock Integrity in SAGD Operations. In SPE Heavy Oil Conference, Calgary, Alberta, 11-13 June. SPE-165422.

Ramamurthy, T. 1993. Strength and Modulus Responses of Transversely Isotropic Rocks. *Comprehensive Rock Engineering*, Vol. 1, pp. 313-329 U.K.: Pergamon Press.

Singhal, B.B.S., and Gupta, R.P. 2010. *Applied Hydrogeology of Fractured Rocks*. Springer Science & Business Media, Springer Dordrecht Heidelberg London New York.

Smith, R.J. 1997. *Geomechanical Effects of Cyclic Steam Stimulation on Casing Integrity*. MS thesis, University of Calgary, Calgary, Canada (Fall 1997).

Sone, H. 2012. *Mechanical Properties of Shale Gas Reservoir Rocks and Its Relation to the In-situ Stress Variation Observed in Shale Gas Reservoirs*. PhD thesis, Stanford University, California, US (March 2012).Suncor Energy, 2013. *2013 AER Performance Presentation: Surface Commercial Scheme Approval No. 8668*. Retrieved from http://www.aer.ca/documents/oilsands/insitu-presentations/2013SuncoreMacKayRiver8668.pdf.

Suncor Energy, 2009. *MacKay River Performance Presentation*. Retrieved from http://www.aer.ca/documents/oilsands/in situ-presentations/2009AthabascaSuncorMacKayRiver8668.pdf.

Tsui, P.C., Cruden, D.M., and Thomson, S. 1988. Mesofabric, Microfabric, and Submicrofabric of Ice-Thrust Bedrock, Highvale Mine, Wabamun Lake Area, Alberta. *Canadian Journal of Earth Sciences*, **25**(9): 1420-1431.

Wyllie, D. C., and Mah, C. 2004. *Rock Slope Engineering*. CRC Press, 4th edition.

Wittke, W. 1990. *Rock Mechanics: Theory and Applications with Case Histories*. Springer-Verlag, Berlin.